Human Molecular Genetics, 2022, Vol. 31, 19, 3325–3340
https://doi.org/10.1093/hmg/ddac114
Advance access publication date 23 May 2022
Original Article

SEMA6B variants cause intellectual disability and alter dendritic spine density and axon guidance

Amélie Cordovado[1], Martina Schaettin[2], Médéric Jeanne[1,3], Veranika Panasenkava[1], Anne-Sophie Denommé-Pichon[4,5], Boris Keren[6], Cyril Mignot[6], Martine Doco-Fenzy[7], Lance Rodan[8,9], Keri Ramsey[10], Vinodh Narayanan[10], Julie R. Jones[11], Eloise J. Prijoles[12], Wendy G. Mitchell[13], Jillian R. Ozmore[14], Kali Juliette[15], Erin Torti[16], Elizabeth A. Normand[16], Leslie Granger[17], Andrea K. Petersen[17], Margaret G. Au[18], Juliann P. Matheny[18], Chanika Phornphutkul[19], Mary-Kathryn Chambers[20], Joaquín-Alejandro Fernández-Ramos[21], Eduardo López-Laso[21], Michael C. Kruer[22,23], Somayeh Bakhtiari[22,23], Marcella Zollino[24,25], Manuela Morleo[26,27], Giuseppe Marangi[24,25], Davide Mei[28], Tiziana Pisano[28], Renzo Guerrini[28], Raymond J. Louie[11], Anna Childers[11], David B. Everman[11], Betrand Isidor[29], Séverine Audebert-Bellanger[30], Sylvie Odent[31], Dominique Bonneau[32], Brigitte Gilbert-Dussardier[33], Richard Redon[34], Stéphane Bézieau[34,35], Frédéric Laumonnier[1], Esther T. Stoeckli[2], Annick Toutain[1,3,*] and Marie-Laure Vuillaume[1,3]

[1]UMR 1253, iBrain, University of Tours, INSERM, Tours 37032, France
[2]Department of Molecular Life Sciences, Neuroscience Center Zurich, University of Zurich, Zurich 8057, Switzerland
[3]Genetics Department, University Hospital of Tours, Tours 37044, France
[4]Functional Unit in Innovative Genomic Diagnosis of Rare Diseases, FHU-TRANSLAD, Dijon-Bourgogne University Hospital, Dijon 21079, France
[5]UMR1231 GAD, INSERM - Bourgogne-Franche Comté University, Dijon 21000, France
[6]Genetics Department, Pitié-Salpêtrière Hospital, AP-HP. Sorbonne University, Paris 75651, France
[7]University Hospital Reims, AMH2, Genetics Division, SFR CAP santé EA3801, Reims 51100, France
[8]Division of Genetics and Genomics, Department of Pediatrics, Boston Children's Hospital, Boston, MA 02115, USA
[9]Department of Neurology, Boston Children's Hospital, Boston, MA 02115, USA
[10]Center for Rare Childhood Disorders, Translational Genomics Research Institute, Phoenix, AZ 85012, USA
[11]Molecular Diagnostic Laboratory, Greenwood Genetic Center, Greenwood, SC 29646, USA
[12]Greenwood Genetic Center, Greenwood, SC 29646, USA
[13]Neurology Division, Keck School of Medicine, University of Southern California, Children's Hospital Los Angeles, CA 90027, USA
[14]Dartmouth Hitchcock Medical Center, Lebanon, NH 03766, USA
[15]Neurology Department, Gillette Children's Specialty Healthcare, St Paul, MN 55101, USA
[16]GeneDx, Gaithersburg, MD 20877, USA
[17]Genetics Division, Department of Pediatric Development and Rehabilitation, Randall Children's Hospital, Portland, OR 97227, USA
[18]Department of Genetics and Metabolism, University of Kentucky, Lexington, KY 40536, USA
[19]Division of Human Genetics, Department of Pediatrics, Warren Alpert Medical School of Brown University, Hasbro Children's Hospital, Providence, RI 02903, USA
[20]Division of Genetics, Rhode Island Hospital, Hasbro Children's Hospital, Providence, RI 02903, USA
[21]Pediatric Neurology Unit, Department of Pediatrics, University Hospital Reina Sofía, IMIBIC and CIBERER, Córdoba 14004, Spain
[22]Pediatric Movement Disorders Program, Division of Pediatric Neurology, Barrow Neurological Institute, Phoenix Children's Hospital, Phoenix, AZ 85016, USA
[23]Departments of Child Health, Neurology, and Cellular & Molecular Medicine, and Program in Genetics, University of Arizona College of Medicine–Phoenix, Phoenix, AZ 85004, USA
[24]Università Cattolica Sacro Cuore, Dipartimento Scienze della Vita e Sanità Pubblica, Sezione di Medicina Genomica, Roma 00168, Italy
[25]Fondazione Policlinico A. Gemelli IRCCS, U. O. C. Genetica Medica, Roma 00168, Italy
[26]Telethon Institute of Genetics and Medicine (TIGEM), Pozzuoli, Naples 80078, Italy
[27]Department of Precision Medicine, University of Campania 'Luigi Vanvitelli', Naples 80138, Italy
[28]Pediatric Neurology, Neurogenetics and Neurobiology Unit and Laboratories, Meyer Children's Hospital, Member of ERN Epicare, University of Florence, Florence 50139, Italy
[29]Medical Genetics Service, Clinical Genetics Unit, University Hospital of Nantes, Hôtel Dieu, Nantes 44093, France
[30]Clinical Genetics Service, University Hospital of Brest, Morvan Hospital, Brest 29609, France
[31]Clinical Genetics Service, University Hospital, Genetic and Development Institute of Rennes IGDR, UMR 6290 University of Rennes, ITHACA ERN, Rennes 35203, France
[32]Department of Medical Genetics, University Hospital of Angers and Mitovasc INSERM 1083, CNRS 6015, Angers 49000, France
[33]Medical Genetics, University Hospital, La Milétrie, BP 577, Poitiers 86021, France
[34]INSERM, CNRS, UNIV Nantes, Thorax Institute, Nantes 44007, France
[35]Medical Genetics Service, University Hospital of Nantes, Nantes 44093, France

*To whom correspondence should be addressed at: Genetics Department, University Hospital, 2 boulevard Tonnellé, Cedex 9, Tours 37044, France. Tel: +33 247478850; Fax: +33 247478653; Email: annick.toutain@univ-tours.fr

Abstract

Intellectual disability (ID) is a neurodevelopmental disorder frequently caused by monogenic defects. In this study, we collected 14 *SEMA6B* heterozygous variants in 16 unrelated patients referred for ID to different centers. Whereas, until now, *SEMA6B* variants

Received: March 14, 2022. **Revised:** April 25, 2022. **Accepted:** May 12, 2022

have mainly been reported in patients with progressive myoclonic epilepsy, our study indicates that the clinical spectrum is wider and also includes non-syndromic ID without epilepsy or myoclonus. To assess the pathogenicity of these variants, selected mutated forms of *Sema6b* were overexpressed in Human Embryonic Kidney 293T (HEK293T) cells and in primary neuronal cultures. shRNAs targeting *Sema6b* were also used in neuronal cultures to measure the impact of the decreased *Sema6b* expression on morphogenesis and synaptogenesis. The overexpression of some variants leads to a subcellular mislocalization of SEMA6B protein in HEK293T cells and to a reduced spine density owing to loss of mature spines in neuronal cultures. *Sema6b* knockdown also impairs spine density and spine maturation. In addition, we conducted *in vivo* rescue experiments in chicken embryos with the selected mutated forms of *Sema6b* expressed in commissural neurons after knockdown of endogenous *SEMA6B*. We observed that expression of these variants in commissural neurons fails to rescue the normal axon pathway. In conclusion, identification of *SEMA6B* variants in patients presenting with an overlapping phenotype with ID and functional studies highlight the important role of SEMA6B in neuronal development, notably in spine formation and maturation and in axon guidance. This study adds *SEMA6B* to the list of ID-related genes.

Graphical Abstract

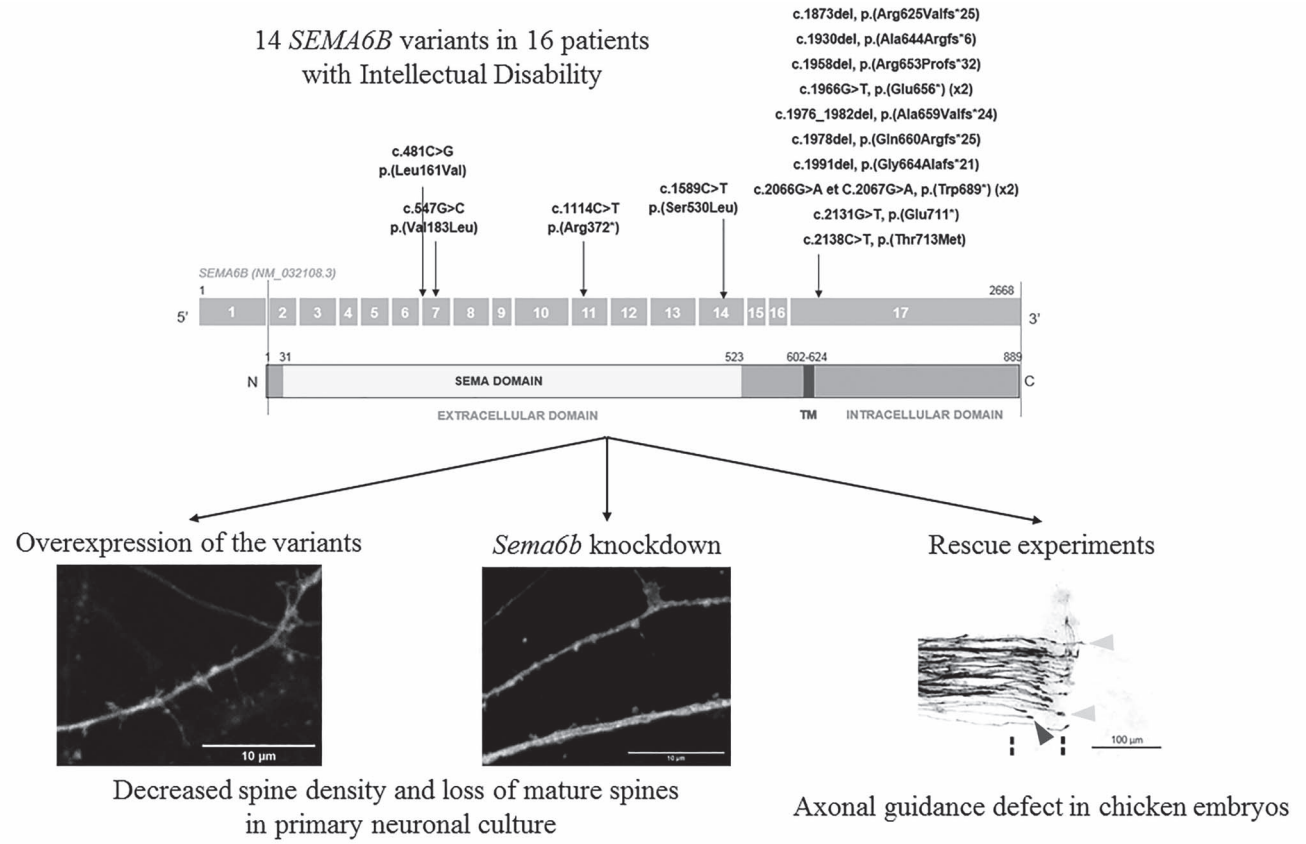

Introduction

Intellectual disability (ID) is a neurodevelopmental disorder characterized by significant limitations in intellectual functioning and adaptive behavior, affecting 2–3% of the general population. The recent advances in high-throughput sequencing technologies have allowed major progress in gene identification and have highlighted the role of *de novo* variants in the pathogenesis of ID (1). Overall, and considering all inheritance patterns, >1500 genes are known to be mutated in ID and almost as many candidate genes could be involved in this highly heterogeneous disorder (SysID database). In a research program dedicated to the identification of novel ID genes, ['Inter-regional Project of the Great Western Exploration Approach for Exome Molecular Causes Severe ID Isolated or Syndromic' (HUGODIMS); Clinical Trials. gov registration no. NCT02136849], we detected a missense variant in the *SEMA6B* gene (semaphorin 6B) in a patient with severe ID, suggesting that this gene may belong to this long list of candidates.

SEMA6B maps to chromosome 19p13.3 and contains 17 exons with a full-length transcript of 3.8 kb (NM_032108.3). It encodes the semaphorin 6B (SEMA6B), a 95.3 kDa transmembrane protein of 888 amino acids that is a member of class 6 semaphorins. Until now, about 30 semaphorins have been described. They are divided into eight subfamilies and share a conserved cysteine-rich extracellular semaphorin domain (2,3). These molecules are involved in axon guidance. They are secreted or membrane-associated glycoproteins able to orchestrate axonal growth in the central nervous system during embryogenesis. Widely expressed in the nervous system, many act as neural chemorepellents for various axon populations and also regulate cell morphology and

motility by modeling the cytoskeleton, the organization of actin filaments and the microtubule network (4). Importantly, class 6 semaphorins can act as ligands and receptors (5,6). A crucial role of SEMA6B has thus been established in central nervous system development as this protein enables axons to find and connect to their targets (7–9). However, its role in ID remains to be functionally characterized.

Until now, *SEMA6B* variants have been identified in individuals with epilepsy, including (1) 10 truncating variants in the last exon of *SEMA6B* in 10 patients with progressive myoclonic epilepsy (PME, MIM #618876) (10–14), and in 1 individual with global developmental delay and recurrent febrile seizures (15) and (2) 1 missense variant in exon 14 in an individual with epilepsy without ID (Supplementary Material, Table S1) (13). Here, we broaden the phenotypic spectrum and the role of *SEMA6B* by reporting 14 heterozygous variants, of which 11 are novel, identified in 16 unrelated patients with moderate to severe ID as well as variable neurological features and seizures in some cases. *SEMA6B* variants were *de novo* in 13 out of 16 patients for whom parental DNA was available. Given the crucial role of SEMA6B in the formation of neural circuits, we hypothesized that *SEMA6B* variants could play a role in the pathophysiology of ID, and we conducted *in vitro* functional studies in Human Embryonic Kidney 293T (HEK293T) cells, in mouse primary hippocampal neurons and *in vivo* in commissural neurons of chicken embryos. We report that the overexpression of the variants and the loss of SEMA6B expression in neuronal cells impair dendritic spine density and maturation. In the absence of endogenous SEMA6B, expression of the *Sema6b* variants in commissural neurons fails to rescue the normal axonal pathway. Axons fail to turn rostrally along the longitudinal axis of the spinal cord. Taken together, these results confirm a role of the identified variants of *SEMA6B* in neural circuit formation which is consistent with the observed phenotypes of the patients.

Results

Description of *SEMA6B* variants

In the present study, 14 *SEMA6B* variants, of which 11 were novel, were identified by exome sequencing in 16 patients with ID. Three of these variants were previously described, c.1976_1982del p.(Ala659Valfs*24) and c.1991del p.(Gly664Alafs*21) in Hamanaka *et al*. (14) and c.2066G>A p.(Trp689*) in Herzog *et al*. (10). A schematic view of the *SEMA6B* gene and the distribution of all variants are presented in Figure 1. All variants reported in the present study were absent in the population database genome aggregation database (gnomAD v2.1.1, 141 456 individuals) except for the missense variant c.1589C>T p.(Ser530Leu) which was found only once out of 209 632 alleles. The nonsense variant c.1114C>T p.(Arg372*) was observed in three unaffected adults in the GeneDx internal database. Recurrence was observed for two frameshift and two nonsense variants considering both the novel and previously described *SEMA6B* variants.

The variants described in the present study occurred *de novo* in 13 patients. Paternal DNA was unavailable for three patients (I-3, I-4 and I-15). Most of the variants (9/14) were nonsense (3/14) and frameshift (6/14), located in the last exon of *SEMA6B* (exon 17) and therefore susceptible to escape the Nonsense-Mediated Decay (NMD) pathway. These variants may lead to the production of a truncated protein lacking the cytoplasmic domain.

Four missense variants were found: two located in exon 7 coding part of the SEMA domain, one located in exon 14 corresponding to the extracellular domain and one located in the last exon corresponding to the intracellular domain. They all were predicted to be pathogenic by most of *in silico* prediction programs (Supplementary Material, Table S2).

For the functional studies, we decided to test one loss-of-function variant in the last exon, escaping NMD [c.2066G>A p.(Trp689*)], which represents the most frequent gene defect described in *SEMA6B* and one missense variant as an example of a novel type of *SEMA6B* mutation [c.547G>C p.(Val183Leu)].

Since the p.(Arg372*) variant is located in exon 11, it probably produces an aberrant transcript degraded by NMD in the patient. However, we could not measure *SEMA6B* mRNA as it is barely detectable in tissues such as peripheral blood cells and fibroblasts (data not shown). We therefore modeled the impact of this variant by using shRNA transfection to knockdown endogenous *Sema6b* expression.

Clinical description

The 16 individuals (I-1–I-16) were aged 6–24 years at the time of reporting and were sporadic cases with no consanguinity (15/15 patients) and of Caucasian origin (13/13), with 1 being partly Native American (Table 1). The reason for referral was known in 15 cases, and in 10 patients, consisted of global delay or ID—associated with epilepsy in four of them—and consisted of autism in 1 patient. Patients I-4 and I-15 were first seen for intractable epilepsy. Patients I-1 and I-3 were initially referred for growth retardation associated with minor congenital anomalies, but I-1 had developmental delay at the first evaluation.

All were born at term or near term. The neonatal period was normal except for patient I-I who had significant feeding difficulties. Birth length and postnatal height were in the normal range for 13/13 patients. Two patients (I-1 and I-3) had a low birth weight and a birth length in the low-normal values, and I-1 still had growth retardation at −3 SD on last examination. A few patients had common digestive problems, mainly gastroesophageal reflux, but no serious medical problem was observed except for two cases of inflammatory bowel disease and one case of early puberty. A retinal dystrophy was suspected in I-1 but was not further documented. None of the patients had visceral or skeletal

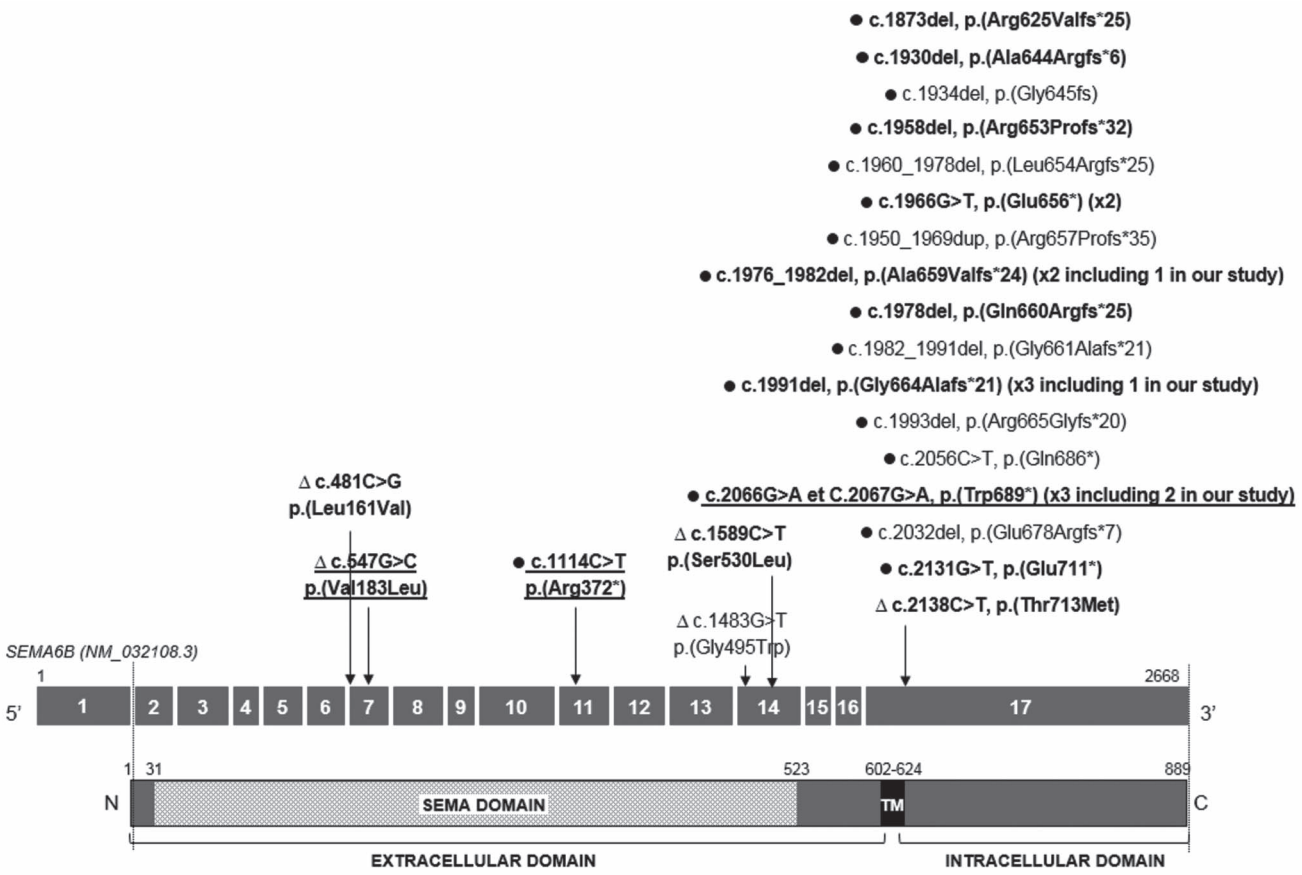

Figure 1. Distribution of *SEMA6B* heterozygous variants. The genomic structure of the *SEMA6B* gene, including 17 exons, is represented. cDNA numbering above *SEMA6B* gene is according to NM_032108. 3. The SEMA6B protein structure is represented below the gene. Amino acid numbers are indicated above the protein. Variants are displayed as changes at DNA (c.) and protein levels (p.). Variants identified in our study are written in bold. The others were described in previous publications (10–15). For recurrent variants, the number of patients reported is indicated in parentheses next to the variant. Triangles and black circles indicate missense and truncating variants (frameshift or nonsense variants), respectively. Variants for which functional studies have been conducted, are underlined. TM: transmembrane domain.

malformations, but 7/13 had orthopedic problems as a consequence of hypotonia, joint laxity or spasticity. Variable dysmorphic features were reported in 11/16 patients, but no consistent morphological phenotype seems to be recognizable.

Fourteen patients had hypotonia in infancy and early childhood and had delayed development. Independent walking was acquired after 18 months in half of the patients and it was difficult with frequent falls in three, and one lost the ability to walk. Two were not able to walk without assistance. Fine motor problems were observed in 14/14 patients and 5/14 had regression of their motor abilities. Language was delayed in 10/12, and on last examination, 6 were non-verbal or had a few words, 4 were able to do short sentences and 6 had simple conversation or were fluent. Only 9/14 were fully toilet-trained (above the age of 4 years in 6 patients). ID of variable degree was observed in 13/14 patients (1 mild, 5 moderate or moderate to severe, 6 severe and 1 profound), and 1 patient was reported as having learning difficulties and followed online school. Autism or autism spectrum disorder (ASD) was diagnosed in 4/15 patients, but 3 others had stereotypies. Behavioral problems were reported in 9/15 patients (including the 4 with ASD) and anxiety was reported in 6/13. Abnormal movements, such as dyskinesia, chorea-like movements and dystonic posturing, were reported in 3 patients, and 10/16 had ataxia or unsteady gait. Tremor and myoclonus were present in 5/12 and 4/11 patients, respectively, but each resolved over time in 1 patient. Half of the patients had pyramidal signs described as spasticity and/or increased/brisk tendon reflexes.

Epilepsy occurred in 13/16 patients, with an age at onset known in 10 cases ranging from 11 months to 5 years (mean = 36 months). Epilepsy consisted in complex partial seizures in three patients, a combination of various types of seizures (myoclonic, atonic, tonic–clonic, tonic and atypical absences) refractory to treatment in four and three patients received a diagnosis of Lennox–Gastaut syndrome. In one of the latter, the diagnosis later changed for Dravet syndrome and then for epileptic encephalopathy. In addition, three patients had non-epileptic drop-attacks. Following the results of exome sequencing compared with their medical history, two patients are now considered as having PME. Epilepsy resolved by the age of 4.5 years in the patient with the

Table 1. Clinical features of the patients carrying a *SEMA6B* variant

Individuals	**I-1**	**I-2**	**I-3**	**I-4**
Gender/age at last examination	M/16 y	M/16 y 3 mo	F/13 y 9 mo	F/9 y
Reason for referral	Growth delay, hypotonia, congenital anomalies	Global delay, ID	Short stature, mild dysmorphic features	Lennox Gastaut syndrome
cDNA variant (NM_032108.3)/Exon	c. 481C > G/exon 7	c. 547G>C/exon 7	c. 1114C>T/exon 11	c. 1589C>T/exon 14
Protein variant	p. (Leu161Val)	p. (Val183Leu)	p. (Arg372*)	p. (Ser530Leu)
Inheritance	*De novo*	*De novo*	Not inherited from the mother	Not inherited from the mother
Delayed development	Y	Y	N	Y
Global/Fine motor problems	Y/Y	Y/Y	N/Y	Y/Y
Language abilities/age at first words	Delay/4 y	≈ 10 words	Sentences/18 mo	2–3 word sentences
Motor regression	Y (wheelchair)	N	N	N
ID degree	Severe	Severe	Learning difficulties	Severe
ASD/stereotypic movements	N/N	N/Y (hand flapping)	N/N	N/N
Behavioral problems/anxiety	N/N	N/Y	N/Y	N/N
Ataxia	Y	Y (not cerebellar)	N	N
Tremor/Myoclonus	N/N	N/N	N/N	N/N
Pyramidal signs	Brisk reflexes, spasticity	Brisk reflexes and spasticity in LL	N	Brisk reflexes
Epilepsy/age at onset/type	N	N	Y/from 18 mo to 4. 5 y	Y/2 y/myoclonic, atypical absences, atonic seizures
Brain MRI anomalies	Cerebellar atrophy, thin corpus callosum, large ventricles, cortical atrophy	Arachnoid cyst, severely stretched out pituitary stalk, mildly short corpus callosum	N	N
Final diagnosis	**ID + neurological signs**	**ID + neurological signs**	**Learning disability + resolving epilepsy**	**ID + epilepsy (Lennox Gastaut)**
Individuals	**I-5**	**I-6**	**I-7**	**I-8**
Gender/age at last examination	M/8 y 11 mo	F/14 y 6 m	M/21 y	F/15 y
Reason for referral	Autism	Global delay, regression, movement disorder	Global delay, multiple congenital anomalies	Developmental delay
cDNA variant (NM_032108.3)/Exon	c. 1873del/exon 17	c. 1930del/exon 17	c. 1958del/exon 17	c. 1966G > T/exon 17
Protein variant	p. (Arg625Valfs*25)	p. (Ala644Argfs*6)	p. (Arg653Profs*32)	p. (Glu656*)
Inheritance	*De novo*	*De novo*	*De novo*	*De novo*
Delayed development	Y	Y	y	Y
Global/fine motor problems	Y/Y	Y/NA	Y/Y	Y/Y
Language abilities/age at first words	Delay/13 mo	2–3 word sentences, dysarthria	Simple conversation	Short sentences
Motor regression	N	Y	N	Y
ID degree	NA	NA	Profound	Severe
ASD/stereotypic movements	Y/Y (hand flapping)	N/N	N/N	Y/N
Behavioral problems/anxiety	Y/Y	Y/N	N/Y	Y/N
Ataxia	N	Y	N	N
Tremor/Myoclonus	N/N	Y (resolved)/NA	N/N	Y/Y
Pyramidal signs	N	Brisk reflexes, spasticity	Brisk reflexes, spasticity	N
Epilepsy/age at onset/type	N	Y/8 y/partial epilepsy	Y/childhood/complex partial seizures	Y/5 y/complex partial seizures
Brain MRI anomalies	NA	N	NA	N
Final diagnosis	**Autism + ID**	**ID + epilepsy + neurological signs**	**ID + epilepsy + neurological signs**	**ID + epilepsy + neurological signs**

(*Continued*)

nonsense variant p.(Arg372*) located in exon 11. It is worthwhile to note that neither of the two patients (both already aged 16 years) with a missense variant in exon 7 had seizures, but one patient with a frameshift variant in exon 17 (p.(Arg625Valfs*25), nearly aged 9 years, did not suffer from epilepsy either.

Head circumference (HC) at birth was in the normal range, mostly in the low-normal values, in seven/eight patients and was above the 95th percentile for one patient. On last examination, 13/14 patients had a HC in the low-normal values (mean at −0.85 SD), with 4 of them being around −2 SD, whereas 1 was at +2.59 SD.

Table 1. Continued

Individuals	**I-9**	**I-10**	**I-11**	**I-12**
Gender/age at last examination	F/20 y	M/21 y	F/16 y	F/6 y
Reason for referral	Global delay	ID, seizures	Severe ID, seizures	NA
cDNA variant (NM_032108.3)/exon	c. 1966G > T/exon 17	c. 1976_1982del/exon 17	c. 1978del/exon 17	c. 1991del/exon 17
Protein variant	p. (Glu656*)	p. (Ala659Valfs*24)	p. (Gln660Argfs*25)	p. (Gly664Alafs*21)
Inheritance	*De novo*	*De novo*	*De novo*	*De novo*
Delayed development	Y	Y	Y	Y
Global/Fine motor problems	Y/Y	Y/Y	Y/NA	Y/Y
Language abilities/age at first words	Simple conversation	Non-verbal	≈ 10 words/3 y	Delay, a few words/2 y
Motor regression	N	Y	N	N
ID degree	Moderate	Severe	Severe	Mild to moderate
ASD/stereotypic movements	N/N	NA/Y	N/NA	Y/Y (hand flapping and clapping)
Behavioral problems/anxiety	Y/Y	Y/NA	NA/NA	ADHD/sensitive to noise
Ataxia	Y	Y	Y	Y
Tremor/Myoclonus	N/Y	Y/N	NA	NA
Pyramidal signs	Increased LL reflexes, spasticity	Brisk reflexes	NA	N
Epilepsy/age at onset/type	Y	Y/3. 5 y	Y/11 mo	Y
Brain MRI anomalies	N	Mild cerebellar atrophy	N	Slightly prominent extra-axial spaces, widened Sylvian fissure
Final Diagnosis	**PME (after ES)**	**ID + epilepsy + neurological signs**	**ID + epilepsy**	**ID + epilepsy (Lennox Gastaut)**
Individuals	**I-13**	**I-14**	**I-15**	**I-16**
Gender/age at last examination	F/15 y	F/16 y	M/15 y 10 mo	F/10 y 8 mo
Reason for referral	ID	Epilepsy, developmental delay	Intractable epileptic encephalopathy	Epilepsy, ID, poor fine motor skills
cDNA variant (NM_032108.3)/Exon	c. 2066G>A/exon 17	c. 2066G>A (mosaic)/exon 17	c. 2131G>T/exon 17	c. 2138C>T/exon 17
Protein variant	p. (Trp689*)	p. (Trp689*)	p. (Glu711*)	p. (Thr713Met)
Inheritance	*De novo*	*De novo*	Not inherited from the mother	*De novo*
Delayed development	Y	Y	Y	N
Global/fine motor problems	Y/Y	Y/Y	Y/Y	N/Y
Language abilities/age at first words	Short sentences/2. 5 y	Fluent/20 mo	A few words	Fluent/10 mo
Motor regression	Y	NA	NA	N
ID degree	Moderate to severe	Moderate	Moderate to severe	Mild
ASD/stereotypic movements	N/N	N/Y (repetitive vocalizations, skin picking)	Y/NA	N/N
Behavioral problems/anxiety	N/N	Hyperphagia/N	Y (aggressive, head banging)/NA	ADHD/Y
Ataxia	Y	Y	Y	N
Tremor/Myoclonus	Y/Y	NA	NA	Y/Y
Pyramidal signs	Increased LL reflexes	NA	NA	N
Epilepsy/age at onset/type	Y	Y/4. 5 y/Myoclonic, tonic, tonic–clonic, atonic seizures, medically refractory	Y/2 y/refractory GTC, myoclonic and focal seizures	Y/5y/refractory myoclonic-atonic, absence, GTC and tonic seizures
Brain MRI anomalies	N	N	N	Arachnoid cyst
Final diagnosis	**PME (when awaiting results of ES)**	**ID + epilepsy + neurological signs**	**Epileptic encephalopathy**	**ID + myoclonic-astatic epilepsy + neurological signs**

GTC: generalized tonic–clonic; LL: lower limbs; mo: months; NA: not available; N: no; y: years; Y: yes.

Brain MRI abnormalities were reported in 5/14 patients and consisted of arachnoid cyst, increased extrafluid spaces and/or cerebral ventricles probably related to some degree of cortical atrophy, cerebellar atrophy, thin

or short corpus callosum and severely stretched out pituitary stalk in one patient with growth hormone deficiency.

Expression and subcellular localization of wild-type and SEMA6B mutants

Wild-type and mutant forms of *Sema6b* were overexpressed first in HEK293T cells in order to assess whether these variants could disturb *Sema6b* expression, stability or its subcellular localization. Wild-type and mutant forms of *Sema6b* were all expressed at the RNA level and at the protein level (Supplementary Material, Fig. S1). Proteins seemed to be present in equal quantity ($P = 0.3918$) in HEK293T cells (Supplementary Material, Fig. S1), suggesting that the mutant proteins are produced and stable. The nonsense variant leads to the production of truncated proteins with the predicted size of 75 kDa. As expected for a transmembrane protein, the wild-type protein when overexpressed was located at the plasma membrane and more precisely at the protrusions or pseudopods of the cells. The mutant form of SEMA6B overexpressing the missense variant p.(Val183Leu) presented the same localization. Surprisingly, the mutant form of SEMA6B overexpressing the nonsense variant p.(Trp689*), expected to be present at the plasma membrane as the truncation appears downstream of the transmembrane domain, was only partially present at the plasma membrane and was also partially retained in the cell (Fig. 2). Co-localization of SEMA6B with a marker of the plasma membrane, a sodium potassium ATPase, was decreased with overexpression of the nonsense variant (Fig. 2).

The wild-type and mutant forms of *Sema6b* were next overexpressed in primary hippocampal neuronal cultures. SEMA6B was located in the three main parts of the neurons (dendrites, axon and soma) whatever the condition (overexpression of the wild-type form or mutant forms of SEMA6B) (Supplementary Material, Fig. S2).

Spine density and spine maturation are reduced with overexpression of *Sema6b* variants

The impact of the wild-type and mutant forms of *Sema6b* on neuronal development and morphology was assessed by measuring the branching complexity and the spine density. Overexpression of the different variants did not affect neuronal morphology, dendritic growth and branching complexity (data not shown) but had an impact on spine density. The variants p.(Val183Leu) and p.(Trp689*) led to a decrease of the total spine number compared with the wild-type. They also induced a decrease in the number of mature spines and a change in the ratio between mature and immature spines (Fig. 3A and B). Taken together, these findings suggest that SEMA6B plays an important role in the formation and the maturation of dendritic spines.

Spine density and spine maturation are reduced after down-regulation of *Sema6b* expression

The transfection of the effective shRNA in Neuro-2a cells resulted in a 54% reduction of *Sema6b* mRNA expression level (data not shown). Effective shRNAs were then transfected in neuronal primary cultures to assess the impact of decreased *Sema6b* expression on spine density. Removing SEMA6B from hippocampal neurons *in vitro* resulted in a reduction of the number of spines (Fig. 4A and B). This reduction was mainly owing to a loss of mature spines, as the number of immature spines was not different from controls.

The *SEMA6B* variants are unable to support axonal navigation during neural circuit formation

Sema6B was previously shown to be required for axon guidance across the midline (9). Therefore, we analyzed whether the truncating mutants or the p.(Val183Leu) mutant were able to rescue axonal pathfinding. To this end, we silenced endogenous chicken SEMA6B with dsRNA derived from the 3'untranslated region (UTR). As expected and shown previously (9), absence of SEMA6B interfered with the navigation of commissural axons across the floorplate, the ventral midline of the spinal cord (Fig. 5A), as only $30.4 \pm 7.6\%$ of the DiI injection sites showed normal axonal trajectories after silencing *SEMA6B*. In control embryos, injected and electroporated with the EGFP-encoding plasmid only, $74.0 \pm 7.0\%$ of the DiI injection sites showed normal axonal trajectories. Co-injection and electroporation of a plasmid encoding wild-type mouse SEMA6B rescued axonal pathfinding, as under these conditions $83.7 \pm 4.9\%$ of the DiI injection sites exhibited normal trajectories. This was not different from the values for the control group. However, none of the variants was able to rescue aberrant axon guidance, as we found only $24.2 \pm 12.1\%$ DiI injection sites with normal trajectories after co-injection of p.(Val183Leu). Similarly, the values for p.(Trp689*) were $21.9 \pm 9.$ 3%. There was no qualitative difference between the phenotypes (Fig. 5B and Supplementary Material, Fig. S3). None of the variants was able to fully or partially rescue the aberrant axonal pathfinding seen after silencing SEMA6B. In contrast to axonal trajectories in control embryos (Fig. 5B), where axons cross the midline and turn rostrally along the contralateral floorplate border, axons failed to cross the floorplate and to turn rostrally in the absence of SEMA6B. The aberrant phenotypes were still found after co-injection of plasmids encoding the *Sema6B* variants but not after the co-injection and electroporation of wild-type *Sema6B*.

Discussion

With 14 variants, of which 11 are novel, added to those already reported in the literature (10–15), our study leads to a total of 22 heterozygous variants currently identified

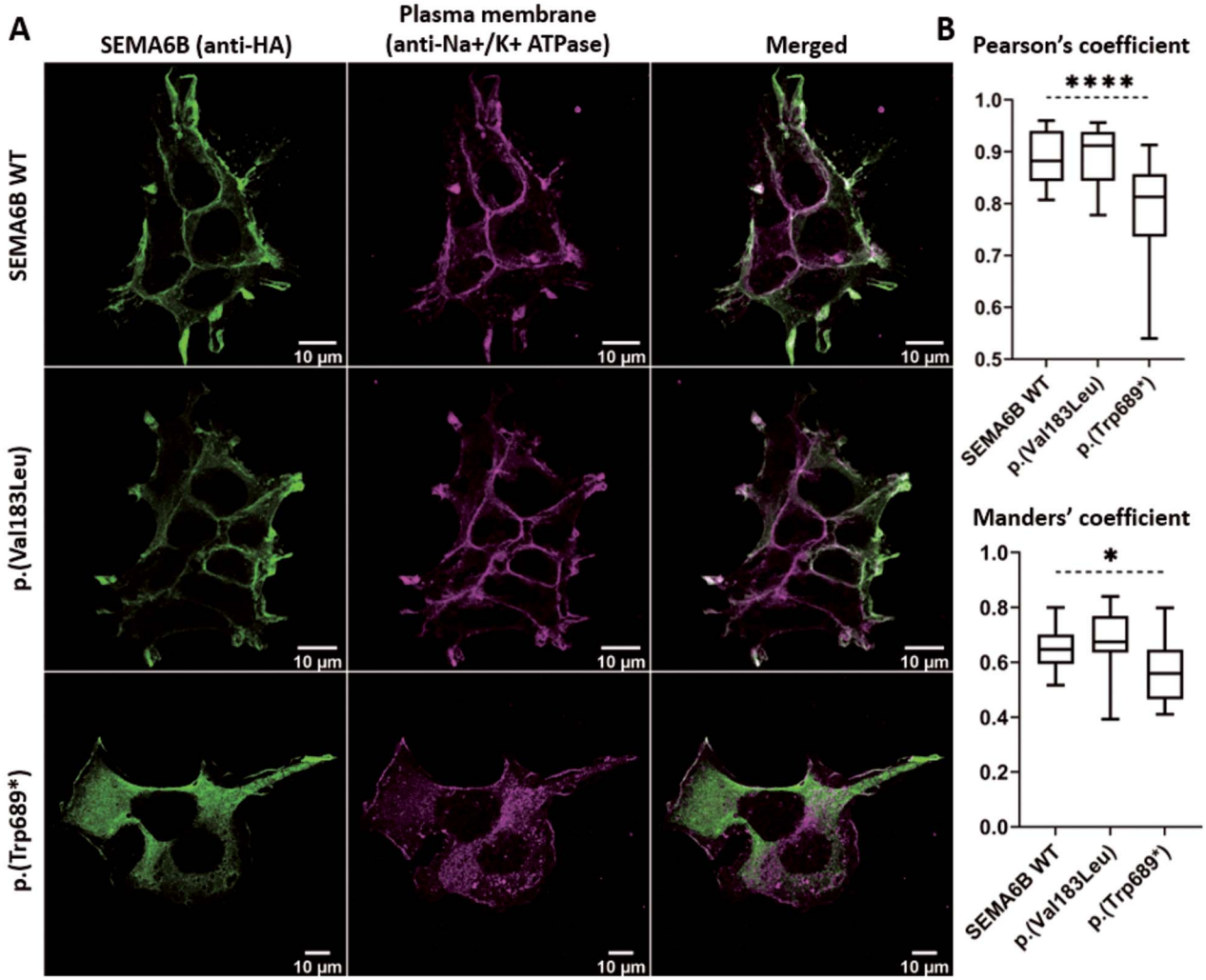

Figure 2. Subcellular localization of wild-type or mutants forms of SEMA6B protein overexpressed in HEK293T cells. (**A**) Confocal images showing SEMA6B localization (magenta) in HEK293T cells after overexpression of SEMA6B variants or wild-type forms. Plasma membrane is shown in green. (**B**) Co-localization was quantified on median projections using JaCop plugin from the ImageJ software based on Pearson's correlation coefficient and Mander's coefficient. Data shown are median, first and third quartiles, minimal and maximal values. More than 23 cells from two independent experiments were analyzed. Statistical analysis was performed with the GraphPad Prism 8.0 software (La Jolla, CA, USA) by using a Kruskal-Wallis test; *$P < 0.05$, ****$P < 0.0001$.

in *SEMA6B* in 28 unrelated patients. In all patients for whom DNA of the two parents was available (22/28), these variants had occurred *de novo*. The vast majority consists of truncating variants (17/22), mostly frameshift (12) or nonsense (5), compared with only 5 missense (Fig. 1). Four of them were recurrent and were observed in different ethnic backgrounds (Supplementary Material, Table S1). In previous reports, all but one were truncating variants located in the last exon, which encodes the intracellular domain of the protein, whereas the sole missense variant was located in exon 14. This could have suggested a particular molecular mechanism leading to a preferential type of pathogenic variants in this region. However, we also found a missense in exon 17 and a nonsense in exon 11. The high proportion of pathogenic variants in the last exon (17/22) is probably not only related to the size of this exon, which is the largest of the gene (926 bp, i.e. 34% of the coding sequence).

Pathogenic variants in *SEMA6B* have been first identified in patients with epilepsy, mainly PME (14), a condition characterized by myoclonus, epilepsy, motor and cognitive decline, and other neurological signs such as ataxia, dysarthria, tremor, spasticity. Our study shows that the *SEMA6B*-related phenotype is wider than previously recognized as none of the 15 patients for whom we had the information was referred with this diagnosis. PME has been finally considered or recognized after the results of exome sequencing in only two patients, although several patients with ID and epilepsy had various neurological signs in common with PME, mainly ataxia or spasticity, or regression of their motor and cognitive abilities. Other patients presented with ID and refractory epilepsy, suggesting that *SEMA6B* should be added to the panel of epileptic encephalopathy genes. In contrast, epilepsy was not observed in three patients, although we cannot totally exclude that it

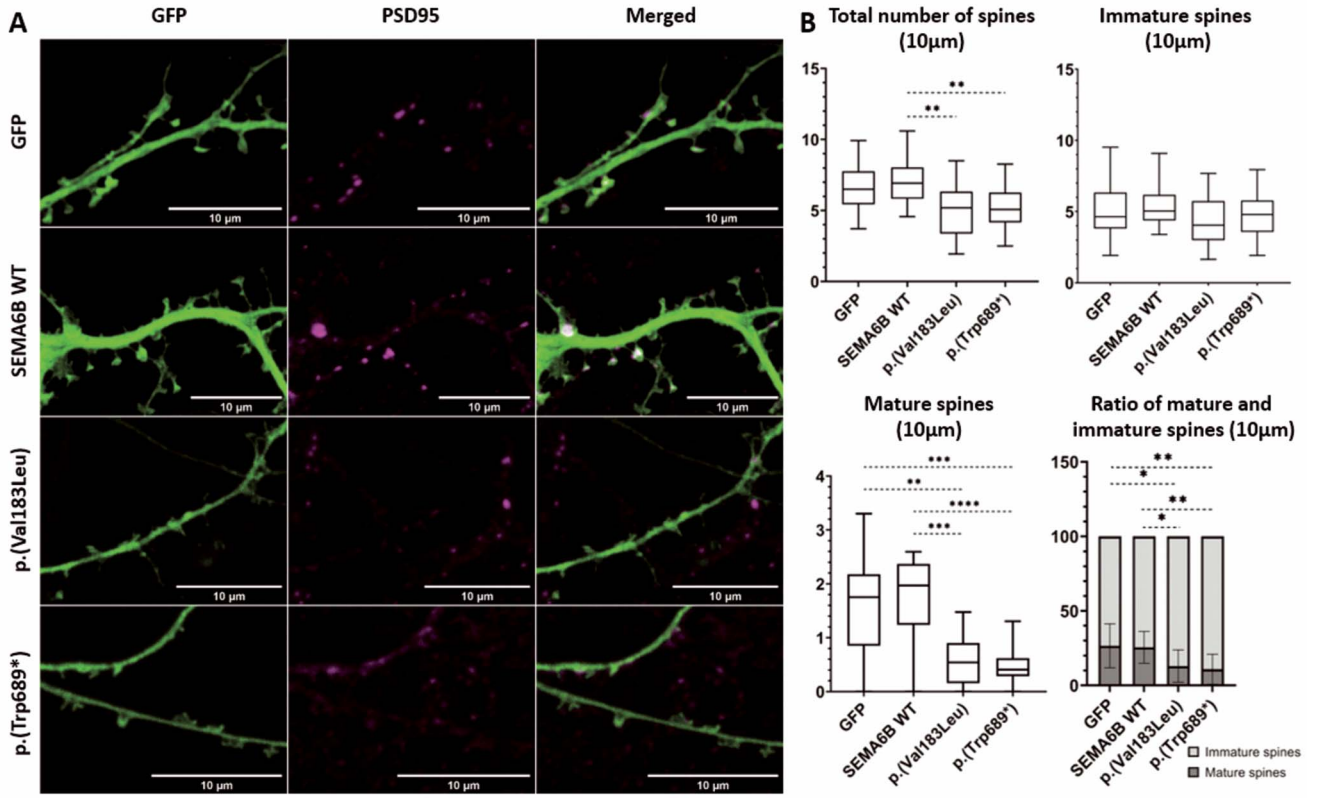

Figure 3. Altered spine density of primary hippocampal neurons after overexpression of *Sema6b* variants. (**A**) The EGFP protein was used to show spine morphology (x63 objective, Scale bar: 10 μm). PSD95 in magenta is used to show post-synaptic density of dendritic spines. SEMA6B transfection of every neuron has been checked before image generation. (**B**) Quantification of spine number per 10 μm of dendrite for each condition. Mature and immature spines were differentiated according to their head diameter (>0.6 μm for mature spines and <0.6 μm for immature spines). Three independent experiments were conducted, leading to the analysis of >16 neurons for each condition. Means +/−SD are represented on the graph presenting the ratio of mature and immature spines. Median, first and third quartiles, minimal and maximal values are represented on the other graphs. Statistical analysis was done by using a Kruskal-Wallis test with the GraphPad Prism 8.0 software (La Jolla, CA, USA): *$P < 0.05$, **$P < 0.01$, ***$P < 0.001$, ****$P < 0.0001$.

will occur later in life. This observation and the fact that the reason for referral in our series was mostly global delay or ID indicate that *SEMA6B* is a gene to consider not only when dealing with severe epilepsy but more generally in neurodevelopment disorders. Previous reports suggested a strong genotype–phenotype correlation, as all truncating variants in the last exon were associated with a severe phenotype, mainly PME, observed in 9 of the 11 patients for whom clinical data were available, or severe ID with early onset recurrent febrile seizures in 1 patient, whereas the missense variant in exon 14 was seen in a patient with epilepsy but normal development (Supplementary Table 1). Although the number of patients with variants outside exon 17 is still limited, our results seem to confirm that patients with truncating variants in the last exon are the most susceptible to manifest PME or refractory epilepsy. In particular, none of the two patients with a missense in exon 7 had epilepsy at the age of 16 years. However, two patients with a missense variant, one in exon 17 but the other in exon 14, also had severe epilepsy. Finally, we did not see significant clinical differences between patients bearing the same recurrent variant.

To assess the involvement of the *SEMA6B* variations in these phenotypes, we performed several functional analyses, notably in primary hippocampal neurons from mouse embryos and in commissural neurons of chicken embryos.

Our *in vitro* data indicate first that overexpression of the variants tested, p.(Val183leu) and p.(Trp689*), do not disturb the SEMA6B synthesis and stability in HEK293T cells. However, the nonsense variant seems to partially prevent the truncated SEMA6B protein from reaching the plasma membrane, whereas the missense variant does not change SEMA6B subcellular distribution. These results are in agreement with the work of Xiaozhen *et al.* (13), showing that another SEMA6B nonsense variant (p.Gln686*) produced a truncated protein which also failed to reach the plasma membrane in HEK293T cells.

Our functional studies validate the pathogenicity of the two variants, p.(Val183Leu) and p.(Trp689*), as their overexpression affects spine density and spine maturation of neurons. Moreover, these two variants are also unable to rescue the aberrant axonal pathfinding seen after silencing SEMA6B in the commissural neurons of chicken. In line with the finding that SEMA6B acts as a

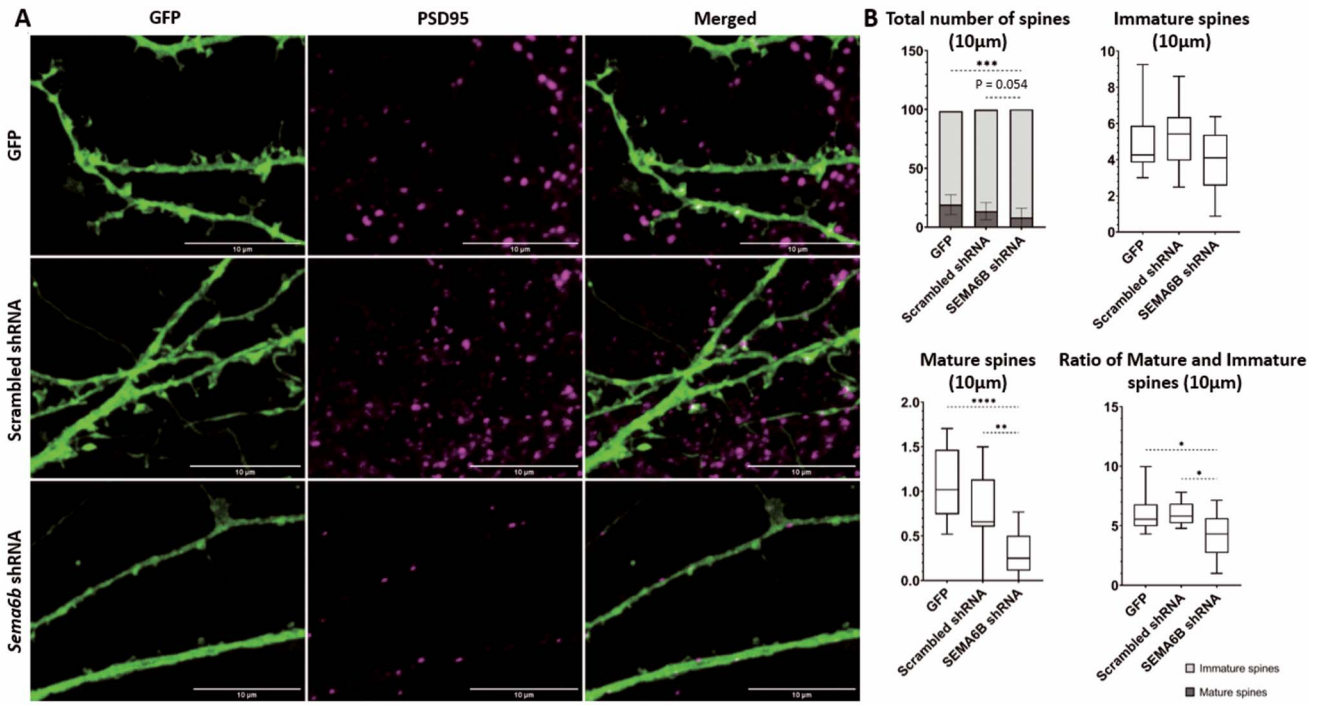

Figure 4. Altered spine density of primary hippocampal neurons after inhibition of *Sema6b* expression. (**A**) The EGFP protein was used to show spine morphology (x63 objective, Scale bar: 10 μm). PSD95 in purple is used to show post-synaptic density of dendritic spines. (**B**) Quantification of spine number per 10 μm of dendrite for each condition. Mature and immature spines were differentiated according to their head diameter (>0.6 μm for mature spines and <0.6 μm for immature spines). Three independent experiments have been done leading to the analysis of >17 neurons for each condition. Means +/−SD are represented on the graphs. Statistical analysis was done by using a Kruskal-Wallis test with the GraphPad Prism 8.0 software (La Jolla, CA, USA): *$P < 0.05$, **$P < 0.01$, ***$P < 0.001$, ****$P < 0.0001$.

receptor in neural circuit formation, mutations resulting in truncation of the cytoplasmic domain could prevent binding of signaling molecules to SEMA6B. The variant p.(Val183Leu) has a transmembrane domain and a normal cytoplasmic domain, and therefore, would not necessarily be non-functional. However, the variant is located in an area of the protein that is required for the interaction with PlexinA2 (16,17). Because the interaction between PlexinA2 and class-6 semaphorins in *cis*, that is in the plane of the same membrane, has been demonstrated to be crucial for axonal targeting (5,9) and, at least indirectly, for spine formation (3,4), the ability of p.(Val183Leu) to form *cis*-interactions could be modified in hippocampal neurons. Our study demonstrates a role of SEMA6B in dendritic spine development and maturation. Several observations indicate that semaphorins are, in general, known contributors of formation (18–20), maturation (21,22), regulation (23,24) and renewal of spines both in development and mature brain (25). Semaphorins also contain a PDZ-binding motif, which allows them to interact with proteins from the postsynaptic density such as PSD-95 (26–28). This interaction enables the semaphorins and their receptors to localize at synapses (29). Effects of semaphorins on dendritic spines seem to be specific to each class or subclass of semaphorin, to neuronal type and depend on the endogenous action of the semaphorin, if it is expressed in the neurons, or on their external action, if they are found in the media surrounding the neurons. A disruption of one of these pathways mediated by the semaphorins may lead to a default in circuit formation and/or in synaptic transmission or network excitability associated to neurodevelopmental diseases.

Interpretation of the nonsense heterozygous variant, c.1114C>T p.(Arg372*), located far upstream of the last exon-exon junction remains challenging. Indeed, the phenotype of the patient is non-specific and less severe. This patient (I-3) is the only one who had learning difficulties but was not formally considered as having ID, and epilepsy resolved by the age of 4–5 years. Moreover, the DNA of the father was unavailable for this patient and this variant was found three times in GeneDx internal database. This variant is predicted to induce NMD leading to the loss of the corresponding truncated transcript. However, even if our *in vitro* analyses suggest that a decreased SEMA6B level impairs dendritic spine density in neuronal cells, these findings remain difficult to interpret in light of what happens in humans. On the one hand, a single copy of *SEMA6B* could be sufficient to maintain SEMA6B function, especially as *SEMA6B* has a low probability of being loss of function intolerant (pLI = 0.06 in GnomAD v2.1.1). On the other hand, a mechanism of genetic compensation cannot be excluded. Through this mechanism, nonsense mutations might lead to upregulation of related genes which can themselves assume the function of the mutated gene

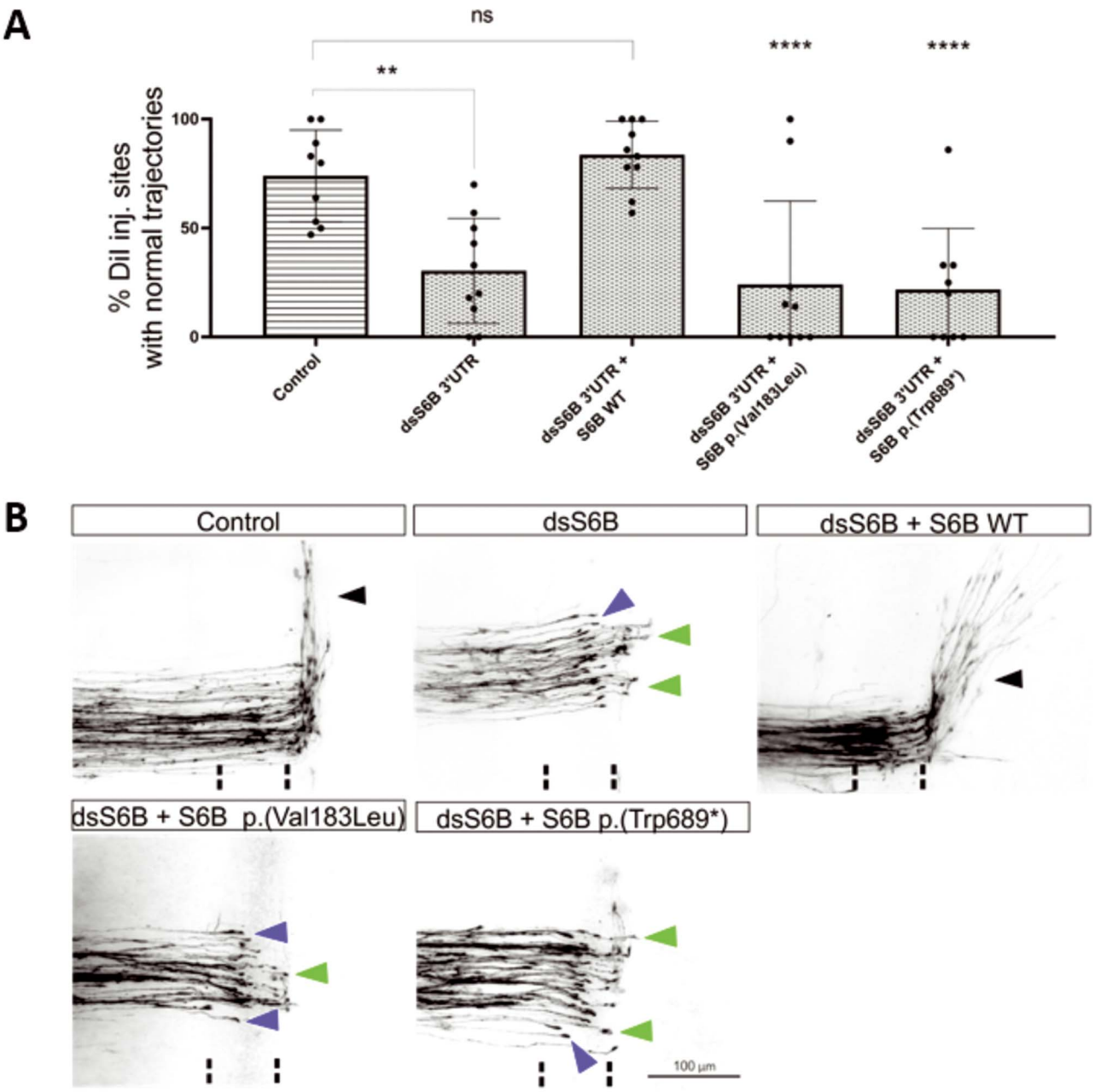

Figure 5. None of the mutant SEMA6B variants can rescue axon guidance. (**A**) Axonal trajectories of dorsal commissural axons were analyzed in control-treated and experimental embryos after silencing SEMA6B using the lipophilic dye DiI to visualize axons in spinal cord whole-mounts. In control-treated embryos, injected only with the EGFP-encoding plasmid, normal trajectories of commissural axons were seen at 74.0 ± 7.0% of the DiI sites ($N = 9$ embryos with a total of $n = 95$ DiI injection sites). After silencing SEMA6B with dsRNA derived from the 3'UTR, normal trajectories were only seen at 30.4 ± 7.6% of the DiI injection sites ($N = 10$; $n = 82$). Axon guidance was restored to normal levels when a plasmid encoding wild-type *Sema6B* was co-injected with the dsRNA (83.7 ± 4.9%; $N = 10$; $n = 101$). Neither co-injection of the p.(Val183Leu) variant (24.2 ± 12.1%; $N = 10$; $n = 92$), nor the co-injection of the variant p.(Trp689*) (21.9 ± 9.3%; $N = 9$; $n = 64$) was able to restore normal axon pathfinding. (**B**) Dorsal commissural axons in control-treated embryos crossed the floorplate (indicated by dashed lines) and turned rostrally along the contralateral floorplate border (black arrowhead). After silencing *SEMA6B* with dsRNA derived from the 3'UTR, axons stalled in the floorplate (blue arrowhead) or failed to turn along the contralateral floorplate border (green arrowhead). This aberrant axonal pathfinding behavior was rescued by co-injection and electroporation of the *SEMA6B* ORF, which was not sensitive to the dsRNA from the 3'UTR. None of the variants was able to rescue aberrant axon guidance.

(30). This dosage compensation mechanism which is not observe *in vitro* after gene knockdown (31) could explain, in humans, mild or non-penetrant phenotype associated with truncating variants located in the NMD-sensitive region. Moreover, it is very likely that truncating variants of the last exon, as they do not induce NMD, lead to a dominant negative effect which can explain the more severe and homogeneous phenotype observed with these variants compared with the milder phenotype associated with the nonsense p.(Arg372*) variant.

In conclusion, our study expands the mutational and clinical spectrum associated with *SEMA6B* variations. This study confirms that loss-of-function variants in the last exon confer pathogenicity and shows that missense mutations also exert deleterious effects. Finally, SEMA6B plays an essential role in neuronal development, notably in spine formation and maturation in addition to its well-known role in axon guidance.

Materials and Methods

Inclusion of patients and genetic analyses

Affected individuals included in the present study were enrolled together with their healthy biological parents in different programs or centers investigating the molecular basis of developmental disorders in a research or clinical setting and were gathered through the GeneMatcher platform (32). If done in a research setting, the studies were approved by local institutional review boards. Written informed consent was obtained from the patient's legal guardians. Clinical information was obtained by review of medical records and the affected individuals' examination. Routine clinical, genetic and metabolic screenings performed during initial workup were negative in each case, which allowed further investigation and exome sequencing.

Rare heterozygous variants were selected according to their *de novo* occurrence if known, their absence in the population database gnomAD v2. 1. 1 and their predicted deleterious effect on the protein.

In silico prediction was performed with Sorting Intolerant From Tolerant (SIFT4G) (33), PolyPhen-2 HumVar (34), MutationTaster (35), Combined Annotation Dependent Depletion (36). Interpretation of the variants was done according to the recommendations of the American College of Medical Genetics and Genomics (37).

The variants described in this study were submitted to the ClinVar database (https://www.ncbi.nlm.nih.gov/clinvar/).

Sema6b expression plasmids and site-directed mutagenesis

Experiments were performed using a pCAG expression plasmid containing the full-length *Sema6b* mouse cDNA sequence (NM_032108. 3) fused to an human influenza hemagglutinin (HA) tag. Human and mouse *SEMA6B* cDNA sequences were compared using nBLAST tool to check the conservation between these two sequences. Eighty-two percent of identity was obtained between the two sequences. Amino acids and nucleotides modified by our *SEMA6B* variations are conserved between human and mouse. *Sema6b* cDNA was amplified by PCR and inserted into a pCR-Blunt II-TOPO (Zero Blunt TOPO PCR Cloning Kit, Invitrogen) cloning vector. The missense variant p.(Val183Leu) was generated by site-directed mutagenesis with the Q5 Site-Directed Mutagenesis kit (New England Biolabs). The oligonucleotides used to generate this missense variant were designed using NEBase Changer and included the following sequences: F-5'ACATGCCAATcTCGCCCTCTTC, R-5'TTGGGGTCATAGGGGCAG. The sequences of all constructs were confirmed by automated DNA Sanger sequencing. Then, the original pCAG expression plasmid and the TOPO plasmids containing the mutated cDNA were cut at the same restriction sites BglII and XbaI to clone back the mutated cDNA insert into the pCAG vector. In order to generate the *Sema6b* constructs containing the nonsense variants p.(Arg372*) or p.(Trp689*), the cDNA located upstream of the variants was amplified by PCR and inserted into the pCAG vector previously cut at BglII and XbaI cloning sites to remove the original *Sema6b* cDNA.

Cell cultures

HEK 293T cell lines [American Type Culture Collection (ATCC), CRL-3216] were cultured and maintained with Dulbecco's Modified Eagle Medium (Gibco, ref 31966047) medium and 10% of fetal bovine serum (FBS; Eurobio, CVFSVF06-01). Neuro-2a cell lines (ATCC, CCL-131) were cultured and maintained with Eagle's Minimum Essential Medium (ATCC, 30-2003) and 10% of FBS.

For primary neuronal cultures, all mouse experiments were performed according to protocols approved by the University of Tours and Institut National de la Santé Et de la Recherche Médicale. Hippocampi were dissected from embryonic day 17 C57BL/6J mouse embryos (Janvier-Labs). The primary neuronal cultures were prepared as previously described (38). Dissociated cells were then plated onto glass coverslips coated in poly-D-lysine (Merk) and laminin (Cat#23017-015, Invitrogen) at a density of 210 cells per mm^2. The cultures were kept in Neurobasal/B-27, and half of the medium was changed twice a week.

RT-PCR and western blot analyses in HEK293T cells

Expression plasmids (wild-type and mutated forms of *Sema6b*) were transfected into HEK293T cells using Lipofectamine 2000 (Invitrogen). RNA was extracted 48 h after transfection using the Direct-Zol RNA Miniprep Plus kit (Zymo Research). Complementary DNA was obtained from 100 ng of mRNA using the sensiFAST cDNA synthesis kit (Meridian Bioscience). Primers were designed with Primer3 (sequences available upon request).

Proteins were extracted using radioimmunoprecipitation assay buffer from Invitrogen. Protein samples were processed for SDS-PAGE at 190 V for 30 min. SDS-PAGE gels were blotted on Nitrocellulose membrane using TransBlot Turbo (Bio-Rad) for 7 min (1. 3A, 25 V). The membrane was blocked for 1 h with 5% milk diluted in Tris buffer saline (TBS)-Tween (1% Tween 20). The membrane was incubated overnight in primary antibody for HA tag (1/500 Cat# 11867423001, Merck) diluted in 5% milk in TBS-Tween buffer. After three 10-min washes with TBS-Tween, the membrane was incubated with a secondary goat horseradish peroxidase

(HRP)-coupled anti-rat antibody (1/10000 Cat#629520, Invitrogen) diluted in 5% milk in TBS-Tween buffer for 1 h at room temperature. The chemiluminescence detection was done using Clarity Western ECL Substrate kit (cat# 1705060, Bio-rad) and the membrane was visualized in a Chemidoc Touch imaging system (Bio-rad). The membrane was then washed three times for 10 min in TBS-Tween and then the secondary antibodies were removed by two washes of 10 min with a stripping buffer (15 g glycine, 1 g SDS, 10 ml Tween20, 1 l water, pH 2. 2), washed again with TBS-Tween and then blocked for 1 h with 5% milk diluted in TBS-Tween. The membrane was incubated 1 h with a mouse antibody targeting GAPDH coupled to HRP (Cat#G9295, Merck) diluted in 5% milk in TBS-Tween buffer, washed three times with TBS-Tween and detection was performed as previously described.

Immunocytochemistry and image analysis in HEK293T cells

Expression plasmids (wild-type and mutated forms of *Sema6b*) were transfected into HEK293T cells using Lipofectamine 2000 (Invitrogen) and HEK293T cells were fixed 48 h later with a solution containing 4% paraformaldehyde/4% sucrose in phosphate buffer saline (PBS). Cultures were then incubated with a blocking buffer (10% donkey serum/0.2% Triton X-100 in PBS) for 1 h, washed with PBS and incubated for 1 h with the following primary antibodies diluted in 3% donkey serum/0.2% Triton X-100 in PBS buffer: rat anti-HA monoclonal antibody (1/200 Cat# 11867423001, Merck) and recombinant rabbit anti-Sodium Potassium ATPase antibody (1/500 Cat#ab76020, Abcam). After several washes in PBS, neurons were incubated for 45 min with the following secondary antibodies diluted in 3% donkey serum/0.2% Triton X-100 in PBS buffer: FluoProbes 488 goat anti-rat Ab (1/500, Cat# A-11006, ThermoFisher) and FluoProbes 594 donkey anti-rabbit Ab (1/500, Cat#FP-SD5110, Interchim). After three washes in PBS, the fixed and stained HEK293T cells were mounted in ProLong Diamond Antifade reagent (Cat# P36391, Invitrogen). Sequential acquisitions were made, and high-resolution z stack images of cells were taken with the x63 objective of a laser-scanning confocal microscope SP-8 (Leica) with optical section separation (z interval) of 0.3 μm. Images were generated by the in-built Leica Application Suite X (Leica). Median projections were made for image analysis. Co-localization quantification was performed using the JACoP plugin of the Fiji software (Wayne Rasband, Bethesda NIH) to obtain Pearson's and Mander's coefficients.

Immunocytochemistry and image analysis of primary neuronal cultures

After transfection with *Sema6b* expression plasmids (wild-type or mutants), neurons were fixed at DIV 6 for subcellular localization analyses and neuronal arborization measurements or at DIV13 for spine density assessment with a solution containing 4% paraformaldehyde/4% sucrose in PBS. After incubation with blocking buffer, fixed neurons were incubated with the monoclonal rat anti-HA antibody (1/200 Cat# 11867423001, Merck) and the mouse anti-PSD95 antibody (1/200, Cat#MA1-046, ThermoFisher) diluted in 3% donkey serum/0.2% Triton X-100 in PBS buffer. After the washes, they were incubated with the secondary antibodies FluoProbes 594 goat anti-rat (1/500, Cat#A110007, Life Technologies) and FluoProbes 680 goat anti-mouse (1/500, Cat#A21057, ThermoFisher) diluted in 3% donkey serum/0.2% Triton X-100 in PBS buffer. After several washes in PBS, the fixed and stained neurons were mounted in ProLong Diamond Antifade reagent (Cat# P36391, Invitrogen). Sequential acquisitions were made, and high-resolution z stack images of neurons were taken with the x63 objective of a laser-scanning confocal microscope SP-8 (Leica) with optical section separation (z interval) of 0.3 μm. SEMA6B transfection of every neuron has been checked before image generation. Images were generated by the in-built Leica Application Suite X (Leica). Maximal projections were made for image production, EGFP labeling was used as a tracer of neuronal and spine morphology and PSD95 was used as a marker of post-synaptic density. The spine density measurements were performed using the Fiji software (Wayne Rasband, Bethesda NIH). Mature spines and immature spines were counted based on their head diameter. Mature spines presented a head diameter of >0.6 μm. Immature spines presented a head diameter of <0.6 μm. Three segments from different dendrites were analyzed for each cell. Quantification was based on three independent experiments with >16 cells of each type analyzed. To measure neuronal arborisation, EGFP was used as a tracer of neuronal morphology. Images were analyzed with the filament tracer plugin of the IMARIS software. Quantification was based on three independent experiments with >20 neurons of each type that were analyzed.

Knockdown experiments

In vitro

Plasmids containing a small hairpin RNA (shRNA) targeting *Sema6b* mouse transcripts as well as plasmids containing a scrambled shRNA were used (cat# MSH073168-CU6 GeneCopoeia). The expression of the shRNA was driven by a U6 promoter. These constructs contained the puromycin resistance gene and an EGFP gene which expresses EGFP protein constitutively in mammalian cells. Both effective shRNA and non-effective shRNA were first transfected in Neuro-2a cells to assess their efficiency to repress the expression of endogenous *Sema6b*. shRNAs were transfected (Lipofectamine 2000, Invitrogen) in Neuro-2a cells 24 h after seeding, and RNA extraction was performed 48 h after transfection using the Direct-Zol RNA Miniprep Plus commercial kit (Zymo Research). Complementary DNA was obtained from 400 ng of mRNA using the PrimeScript RT Reagent Kit (Perfect Real Time) (cat# RR037A, Takara). qPCR experiments were run in duplicates with 500 ng of cDNA on the LightCycler 480 (Roche Diagnostics, Meylan, France) using the SYBR Green Master Mix commercial

kit (Applied Biosystem, Foster City, CA, USA). Relative expression was assessed using the advanced E-method from the LightCycler software (Roche Diagnostics). *Hprt*, *Gapdh* and Beta-actin were used as reference genes for normalization. To measure the expression levels of *Sema6b* in each condition, RT-qPCR analyses were performed on three independent transfections.

Neurons were transfected (Lipofectamine 2000, Invitrogen) at DIV 10 with non-effective or effective shRNA. They were fixed at DIV 13 and spine density measurements were performed as described previously. The EGFP protein was used to show spine morphology. Quantification was based on three independent experiments, leading to >17 cells analyzed for each condition.

In vivo

Silencing of SEMA6B in chicken embryos was done by *in ovo* RNAi, as described previously (39). In brief, fertilized chicken eggs were obtained from a local hatchery (Brüterei Stoeckli, Ohmstal). All experiments, including chicken embryos, were carried out in accordance with Swiss law on animal experimentation and were approved by the cantonal veterinary office of the Canton of Zurich. After 2.5–3 days of incubation at 39°C, eggs were windowed to gain access to the developing embryos for injection and electroporation of dsRNA and/or plasmids. A mix of 350 ng/μl of dsRNA derived from the 3'UTR or the Open Reading Frame (ORF) of SEMA6B and 20 ng/μl βactin-EGFP for transfection control were injected into the central canal of the spinal cord prior to electroporation with five pulses of 50 ms duration at 25 V, as described previously (9,39). The generation of dsRNA was done as described previously (40). For rescue experiments, 300 ng/μl of the respective plasmid (see before) were used for co-injections with the dsRNA and the EGFP plasmid.

We demonstrated that the dsRNA derived from the 3'UTR of SEMA6B was as effective as the dsRNA derived from the ORF that we used in our previous experiments (Andermatt *et al.*) (9). We also verified the suitability of our approach by using dsRNA from the ORF of SEMA6B together with the ORF of wild-type mouse Sema6B. Under these conditions, there was no rescue of the aberrant axon guidance phenotype, as the dsRNA derived from the ORF of chicken SEMA6B did also destroy the mRNA derived from mouse *Sema6B*.

Post-commissural neuron phenotype analysis

Chicken embryos were sacrificed at HH25-26 and the spinal cords were dissected as open-book preparations to label dI1 commissural neurons with the lipophilic dye Fast-DiI (5 mg/ml in ethanol, Molecular Probes) as described previously (39). DiI injection sites were then analyzed by fluorescent microscopy (Olympus DSU coupled to BX61 microscope). An injection site was considered to exhibit a 'floorplate stalling' phenotype when >50% of the axons failed to cross the floorplate and stalled before the exit site. An injection site was considered to show a 'no turn' phenotype when at least 50% of the axons reaching the exit site failed to turn into the longitudinal axis. Note that the 'no turn' phenotype is not independent of the 'floorplate stalling' phenotype because we did not consider injection sites, where <10 fibers reached the exit site. Thus, a strong 'floorplate stalling' phenotype prevented the analysis of the turning phenotype. For this reason, we only compared the DiI injection sites with normal trajectories in our statistical analysis. Images were taken with an Olympus BX61 microscope equipped with a spinning disk unit.

Statistical analysis

To compare variables between subgroups, a Kruskal-Wallis test followed by a Dunn's multiple comparison test were used for *in vitro* studies on HEK293T cells and on primary hippocampal neurons or a one-way ANOVA followed by Tukey's *post hoc* test were used for *in vivo* studies on chicken embryos. A P-value < 0.05 was considered to be significant. Statistical analyses were performed using Prism v8 software (GraphPad).

Supplementary Material

Supplementary Material is available at *HMGJ* online.

Data availability

The authors confirm that the data supporting the findings of this study are available within this article and its supplementary material, or available upon request without undue reservation except for exome sequencing data owing to privacy and ethical restrictions.

Acknowledgements

We would like to thank all the families for participating in this study, Dr Frédérique Allaire from the Health Regional Agency of Poitou-Charentes for supporting this project and Telethon Undiagnosed Diseases Program. We thank the microscopy platform of Tours for their technical assistance. We are grateful to Dr William Dobyns for his help in the interpretation of the brain MRI of patient I-2. Funding for HUGODIMS (Western France exome-based trio approach project to identify genes involved in ID) was supported by a grant from the French Ministry of Health and from the Health Regional Agency from Poitou-Charentes (HUGODIMS, 2013, RC14_0107). A.C. is a research student recipient of a grant from the University of Tours.

Conflict of Interest statement. E.T. and E.A.N. are employees of GeneDx, Inc. The other authors report no competing interests.

Web resources

GeneMatcher, https://genematcher.org/
GnomAD Browser v2. 1. 1, https://gnomad.broadinstitute.org/
OMIM, https://www.omim.org/

SysID database, https://www.sysid.dbmr.unibe. ch/.
NBLAST, https://blast.ncbi.nlm.nih.gov/
Nebase Changer, https://nebasechanger.neb.com
ClinVar, https://www.ncbi.nlm.nih.gov/clinvar/

References

1. Maia, N., Nabais Sá, M.J., Melo-Pires, M., de Brouwer, A.P.M. and Jorge, P. (2021) Intellectual disability genomics, current state, pitfalls and future challenges. *BMC Genom.*, **22**, 909.
2. Yazdani, U. and Terman, J.R. (2006) The semaphorins. *Genome Biol.*, **7**, 211.
3. Pasterkamp, R.J. (2012) Getting neural circuits into shape with semaphorins. *Nat. Rev. Neurosci.*, **13**, 605–618.
4. Jongbloets, B.C. and Pasterkamp, R.J. (2014) *Semaphorin signalling during development*, *Development*, **141**, 3292–3297.
5. Perez-Branguli, F., Zagar, Y., Shanley, D.K., Graef, I.A., Chédotal, A. and Mitchell, K.J. (2016) Reverse signaling by semaphorin-6A regulates cellular aggregation and neuronal morphology. *PLoS One*, **11**, e0158686.
6. Battistini, C. and Tamagnone, L. (2016) Transmembrane semaphorins, forward and reverse signaling, have a look both ways. *Cell. Mol. Life Sci.*, **73**, 1609–1622.
7. Suto, F., Ito, K., Uemura, M., Shimizu, M., Shinkawa, Y., Sanbo, M., Shinoda, T., Tsuboi, M., Takashima, S., Yagi, T. *et al.* (2005) Plexin-A4 mediates axon-repulsive activities of both secreted and transmembrane semaphorins and plays roles in nerve fiber guidance. *J. Neurosci.*, **25**, 3628–3637.
8. Tawarayama, H., Yoshida, Y., Suto, F., Mitchell, K.J. and Fujisawa, H. (2010) Roles of semaphorin-6B and plexin-A2 in lamina-restricted projection of hippocampal mossy fibers. *J. Neurosci.*, **30**, 7049–7060.
9. Andermatt, I., Wilson, N.H., Bergmann, T., Mauti, O., Gesemann, M., Sockanathan, S. and Stoeckli, E.T. (2014) Semaphorin 6B acts as a receptor in post-crossing commissural axon guidance. *Development*, **141**, 3709–3720.
10. Herzog, R., Hellenbroich, Y., Brüggemann, N., Lohmann, K., Grimmel, M., Haack, T.B., Spiczak, S.v. and Münchau, A. (2021) Zonisamide-responsive myoclonus in SEMA6B-associated progressive myoclonic epilepsy. *Ann. Clin. Transl. Neurol.*, **8**, 1524–1527.
11. Li, Q., Liu, M., Huang, D.-P., Li, T., Huang, J., Jiang, P., Ling, W.-H. and Chen, X.-Q. (2021) A de novo SEMA6B variant in a Chinese patient with progressive myoclonic epilepsy-11 and review of the literature. *J. Mol. Neurosci.*, **71**, 1944–1950.
12. Courage, C., Oliver, K.L., Park, E.J., Cameron, J.M., Grabińska, K.A., Muona, M., Canafoglia, L., Gambardella, A., Said, E., Afawi, Z. *et al.* (2021) Progressive myoclonus epilepsies-residual unsolved cases have marked genetic heterogeneity including dolichol-dependent protein glycosylation pathway genes. *Am. J. Hum. Genet.*, **108**, 722–738.
13. Xiaozhen, S., Fan, Y., Fang, Y., Xiaoping, L., Jia, J., Wuhen, X., Xiaojun, T., Jun, S., Yucai, C., Hong, Z. *et al.* (2021) Novel truncating and missense variants in SEMA6B in patients with early-onset epilepsy. *Front. Cell Dev. Biol.*, **9**, 633819.
14. Hamanaka, K., Imagawa, E., Koshimizu, E., Miyatake, S., Tohyama, J., Yamagata, T., Miyauchi, A., Ekhilevitch, N., Nakamura, F., Kawashima, T. *et al.* (2020) De novo truncating variants in the last exon of SEMA6B cause progressive myoclonic epilepsy. *Am. J. Hum. Genet.*, **106**, 549–558.
15. Shu, L., Xu, Y., Tian, Q., Chen, Y., Wang, Y., Xi, H., Wang, H., Xiao, N. and Mao, X. (2021) A frameshift variant in the SEMA6B gene causes global developmental delay and febrile seizures. *Neurosci. Bull.*, **37**, 1357–1360.
16. Janssen, B.J.C., Robinson, R.A., Pérez-Brangulí, F., Bell, C.H., Mitchell, K.J., Siebold, C. and Jones, E.Y. (2010) Structural basis of semaphorin–plexin signalling. *Nature*, **467**, 1118–1122.
17. Rozbesky, D., Verhagen, M.G., Karia, D., Nagy, G.N., Alvarez, L., Robinson, R.A., Harlos, K., Padilla-Parra, S., Pasterkamp, R.J. and Jones, E.Y. (2020) Structural basis of semaphorin-plexin cis interaction. *EMBO J.*, **39**, e102926.
18. Duan, Y., Wang, S.-H., Song, J., Mironova, Y., Ming, G., Kolodkin, A.L. and Giger, R.J. (2014) Semaphorin 5A inhibits synaptogenesis in early postnatal- and adult-born hippocampal dentate granule cells. *elife*, **3**, e04390.
19. Tan, C., Lu, N.-N., Wang, C.-K., Chen, D.-Y., Sun, N.-H., Lyu, H., Körbelin, J., Shi, W.-X., Fukunaga, K., Lu, Y.-M. *et al.* (2019) Endothelium-derived semaphorin 3G regulates hippocampal synaptic structure and plasticity via neuropilin-2/plexinA4. *Neuron*, **101**, 920–937.e13.
20. Paradis, S., Harrar, D.B., Lin, Y., Koon, A.C., Hauser, J.L., Griffith, E.C., Zhu, L., Brass, L.F., Chen, C. and Greenberg, M.E. (2007) An RNAi-based approach identifies molecules required for glutamatergic and GABAergic synapse development. *Neuron*, **53**, 217–232.
21. Morita, A., Yamashita, N., Sasaki, Y., Uchida, Y., Nakajima, O., Nakamura, F., Yagi, T., Taniguchi, M., Usui, H., Katoh-Semba, R. *et al.* (2006) Regulation of dendritic branching and spine maturation by semaphorin3A-Fyn signaling. *J. Neurosci.*, **26**, 2971–2980.
22. Makihara, H., Nakai, S., Ohkubo, W., Yamashita, N., Nakamura, F., Kiyonari, H., Shioi, G., Jitsuki-Takahashi, A., Nakamura, H., Tanaka, F. *et al.* (2016) CRMP1 and CRMP2 have synergistic but distinct roles in dendritic development. *Genes Cells*, **21**, 994–1005.
23. Simonetti, M., Paldy, E., Njoo, C., Bali, K.K., Worzfeld, T., Pitzer, C., Kuner, T., Offermanns, S., Mauceri, D. and Kuner, R. (2021) The impact of semaphorin 4C/plexin-B2 signaling on fear memory via remodeling of neuronal and synaptic morphology. *Mol. Psychiatry*, **26**, 1376–1398.
24. Lin, X., Ogiya, M., Takahara, M., Yamaguchi, W., Furuyama, T., Tanaka, H., Tohyama, M. and Inagaki, S. (2007) Sema4D-plexin-B1 implicated in regulation of dendritic spine density through RhoA/ROCK pathway. *Neurosci. Lett.*, **428**, 1–6.
25. Jongbloets, B.C., Lemstra, S., Schellino, R., Broekhoven, M.H., Parkash, J., Hellemons, A.J.C.G.M., Mao, T., Giacobini, P., van Praag, H., De Marchis, S. *et al.* (2017) Stage-specific functions of semaphorin7A during adult hippocampal neurogenesis rely on distinct receptors. *Nat. Commun.*, **8**, 14666.
26. Burkhardt, C., Müller, M., Badde, A., Garner, C.C., Gundelfinger, E.D. and Püschel, A.W. (2005) Semaphorin 4B interacts with the post-synaptic density protein PSD-95/SAP90 and is recruited to synapses through a C-terminal PDZ-binding motif. *FEBS Lett.*, **579**, 3821–3828.
27. Inagaki, S., Ohoka, Y., Sugimoto, H., Fujioka, S., Amazaki, M., Kurinami, H., Miyazaki, N., Tohyama, M. and Furuyama, T. (2001) Sema4C, a transmembrane semaphorin, interacts with a post-synaptic density protein, PSD-95. *J. Biol. Chem.*, **276**, 9174–9181.
28. Schultze, W., Eulenburg, V., Lessmann, V., Herrmann, L., Dittmar, T., Gundelfinger, E.D., Heumann, R. and Erdmann, K.S. (2001) Semaphorin4F interacts with the synapse-associated protein SAP90/PSD-95. *J. Neurochem.*, **78**, 482–489.
29. Mann, F., Chauvet, S. and Rougon, G. (2007) Semaphorins in development and adult brain: implication for neurological diseases. *Prog. Neurobiol.*, **82**, 57–79.
30. El-Brolosy, M.A., Kontarakis, Z., Rossi, A., Kuenne, C., Günther, S., Fukuda, N., Kikhi, K., Boezio, G.L.M., Takacs, C., Lai, S.-L.

et al. (2019) Genetic compensation triggered by mutant mRNA degradation. *Nature*, **568**, 193–197.
31. Rossi, A., Kontarakis, Z., Gerri, C., Nolte, H., Hölper, S., Krüger, M. and Stainier, D.Y.R. (2015) Genetic compensation induced by deleterious mutations but not gene knockdowns. *Nature*, **524**, 230–233.
32. Sobreira, N., Schiettecatte, F., Valle, D. and Hamosh, A. (2015) GeneMatcher: a matching tool for connecting investigators with an interest in the same gene. *Hum. Mutat.*, **36**, 928–930.
33. Ng, P.C. and Henikoff, S. (2003) SIFT: predicting amino acid changes that affect protein function. *Nucleic Acids Res.*, **31**, 3812–3814.
34. Adzhubei, I.A., Schmidt, S., Peshkin, L., Ramensky, V.E., Gerasimova, A., Bork, P., Kondrashov, A.S. and Sunyaev, S.R. (2010) A method and server for predicting damaging missense mutations. *Nat. Methods*, **7**, 248–249.
35. Schwarz, J.M., Rödelsperger, C., Schuelke, M. and Seelow, D. (2010) MutationTaster evaluates disease-causing potential of sequence alterations. *Nat. Methods*, **7**, 575–576.
36. Rentzsch, P., Schubach, M., Shendure, J. and Kircher, M. (2021) CADD-splice-improving genome-wide variant effect prediction using deep learning-derived splice scores. *Genome Med.*, **13**, 31.
37. Richards, S., Aziz, N., Bale, S., Bick, D., Das, S., Gastier-Foster, J., Grody, W.W., Hegde, M., Lyon, E., Spector, E. *et al.* (2015) Standards and guidelines for the interpretation of sequence variants: a joint consensus recommendation of the American College of Medical Genetics and Genomics and the Association for Molecular Pathology. *Genet. Med.*, **17**, 405–423.
38. Iqbal, Z., Willemsen, M.H., Papon, M.-A., Musante, L., Benevento, M., Hu, H., Venselaar, H., Wissink-Lindhout, W.M., Vulto-van Silfhout, A.T., Vissers, L.E.L.M. *et al.* (2015) Homozygous SLC6A17 mutations cause autosomal-recessive intellectual disability with progressive tremor, speech impairment, and behavioral problems. *Am. J. Hum. Genet.*, **96**, 386–396.
39. Wilson, N.H. and Stoeckli, E.T. (2012) In ovo electroporation of miRNA-based plasmids in the developing neural tube and assessment of phenotypes by DiI injection in open-book preparations. *J. Vis. Exp.*, **68**, e4384.
40. Pekarik, V., Bourikas, D., Miglino, N., Joset, P., Preiswerk, S. and Stoeckli, E.T. (2003) Screening for gene function in chicken embryo using RNAi and electroporation. *Nat. Biotechnol.*, **21**, 93–96.